Journal of Applied Fluid Mechanics, Vol. 18, No. 9, pp. 2321-2331, 2025.
Available online at www.jafmonline.net, ISSN 1735-3572, EISSN 1735-3645.
https://doi.org/10.47176/jafm.18.9.3330

Numerical Study on the Motion and Wave Loads of an Uncrewed Surface Vehicle Catamaran at Low Speed in Sea Waves

T. T. Nguyen[1†], T. L. Phan[1] and T. H. Le[2]

[1] *The University of Danang-University of Science and Technology, Danang City, 50000, Vietnam*
[2] *Ho Chi Minh City University of Technology (HCMUT), VNU-HCM, Ho Chi Minh City, Vietnam*

†*Corresponding Author Email: ntthua@dut.udn.vn*

ABSTRACT

Modern ship designs are being developed for various purposes in uncrewed operation. In particular, low-speed uncrewed surface vehicle (USV) catamarans have been applied as rescued boats in recent years. Therefore, predicting the performance of this ship type in calm water and waves is necessary. This study investigates the response, shear force, and bending moment of a low-speed USV catamaran operating in regular and irregular waves. Numerical simulations are conducted using the Ansys AQWA solver, which employs the boundary element method to model inviscid flow. The catamaran's responses in regular waves, with the ratio of wavelength to ship length ranging from 0.4 to 2.0, are compared with the experimental data. The catamaran's behavior in irregular waves is then determined from integrating its responses in regular waves over the encounter wave spectrum. Additionally, the catamaran's responses and the wave-induced vertical shear force and the bending moment at the x- and y-axes within a frequency range of 0.2 to 3.0 rad/s are analyzed. We demonstrated that the heave, roll, and pitch of the catamaran align well with the corresponding experimental data. Significant vertical shear forces are observed at a wavelength-to-ship-length ratio of 1.0, particularly at one-fourth of the ship's length from either end. The transverse bending moment is significant in a wide range of wave frequencies for the ship in beam seas. The findings show that the maximum midship vertical bending moment in the frequency range of 1.5 to 3.0 when the ship moves in head waves should be considered. The vertical shear force and transverse midship bending moment in the whole frequency domain should be assessed when the catamaran operates in beam waves.

Article History

Received December 28, 2024
Revised March 12, 2025
Accepted April 11, 2025
Available online July 5, 2025

Keywords:

Small uncrewed surface vehicle catamaran
Low speed
Water waves
Ship response
Wave loads

1. INTRODUCTION

Twin hull boats are being developed for various purposes because of their stability during operation. The shape of these vessels is designed to meet the transportation needs and working environment. Many studies have been conducted to predict the motion of catamarans at high speeds in water waves using computational methods and experimental studies. For instance, Bouscasse et al. (2013) studied the motion of a fast catamaran in regular waves, analyzing maximum response, nonlinear effects on the vessel response, and additional resistance.

Durante et al. (2020) conducted an experimental benchmark study of a catamaran in regular and irregular head waves to obtain relevant statistical estimates, validating the wave height, axial force, pitch, roll motion, vertical acceleration of the bridge, and vertical velocity of the flight deck of the ship. In addition, they built a data-driven system trained based on the experimental results of the ship's motion in water waves to predict the ship's temporal response to unseen wave frequencies. The results showed that the predicted motion response of the vessel in head seas and bow seas was similar to the experimental data in the range of long-crested waves.

In a similar study, Matsubara (2011) measured the motion and loads of a large high-speed catamaran using a hydro-elastic segmented model, estimating the vertical bending moment of the ship without slamming influence. The rigid demi-hull as a slamming model was assessed with a forcing oscillatory device. The experimental results demonstrated that the heave and pitch of the ship in regular waves are both strongly nonlinear responses related to the

wave height; the vertical bending moment caused by waves was proportional to the square of the wave height.

Novák (2022) measured the motion of a USV catamaran under rough waves using the state estimation method for experimental data and actual tests. The ship's motion with six degrees of freedom was determined from both methods. The author demonstrated that the state estimation method is more convenient than the actual tests; the results were consistent.

Researchers use the inviscid flow method and three-dimensional (3D) Rankine panel method to predict the seakeeping behavior of ships in both regular and irregular waves. One study predicted the behavior of a high-speed catamaran in waves using 3D translating–pulsating or pulsating source distribution techniques to find the nonlinear effects of water waves (Fang & Chan, 2004). The authors found that the ship motion obtained from both methods agreed with the experimental data except for the numerical results around the resonance of the pitch motions.

Similarly, the seakeeping performance of a catamaran at medium speed was analyzed using the 3D Rankine panel method, comparing the numerical results using SWAN2, MOT35, and NDRIFT codes (Zaraphonities et al., 2015). The ship responses obtained from the codes were consistent except those around the peak value. In related work, the numerical simulations of a ship in deep water and finite water waves were conducted to define ship motion in regular waves (Liu, 2016). The author designed a program for solving the linear seakeeping problem at zero speed based on inviscid flow and the Rankine panel method to calculate the ship motion in the frequency domain. The results extracted from this program were then compared with the numerical results from MAPS0 and WAMIT codes, demonstrating strong agreement with experimental results.

Lin et al. (2017) compared the heave and pitch of a high-speed catamaran obtained from the Rankine panel method, computational fluid dynamics (CFD) method, and experiments. The numerical results from the Rankine panel method showed that the heave response was consistent with the experimental results. However, the pitch responses in the frequency range from 0.7 to 1.1 rad/s differed from the experimental results. The motion response obtained by this method is better than that by the strip method.

In recent years, CFD methods have been widely used to calculate the motion of ships in regular waves. For example, the motion of a double hull at various Froude numbers and lateral separation ratios was analyzed to learn the ship's behavior in water waves and determine the ship's optimal size (Fitriadhy et al., 2017). Sun et al. (2016) employed CFD-based simulation to estimate the heave and pitch responses and resistance of a catamaran with a hard-chine section. In addition, other researchers studied the added resistance of a catamaran in water waves by simulating fluid surrounding the hull (Armstrong and Schmieman, 2005; Vernengo et al., 2021).

The effects of the stern flap on the seakeeping performance of a catamaran in head waves were studied by Wang et al. (2020). Furthermore, the unsteady Reynolds-averaged Navier–Stokes equation method was used to predict the heave and pitch motion of the catamaran under various ship speeds and wave frequencies in head seas at high Froude numbers (Guo et al., 2016). Zhang et al. (2021) predicted the self-propulsion of a catamaran with hydrofoils in regular waves using CFD-based simulation in Star CCM+ solver. They determined the catamaran's heave, pitch, resistance, and velocity for different wave frequencies and heights. Their results showed that the simulated ship behavior agreed with the experimental results; however, the computation was time-consuming, so only some case studies could be simulated.

The catamaran model as a USV is being developed to meet the needs of maritime transport, search, and rescue. The size and speed of the vessel are extended to expand the scope of the model. Numerical studies of large USV motions in 0° and 30° stern oblique waves were performed using CFD (Huang et al., 2021). They analyzed the vehicle's heave, roll, and pitch responses in sea states 5 and 7 water levels and predicted the radiation force, diffraction force, and total drag of the catamaran under various wave conditions. In another study, the actual water waves in the inner region of the USV catamaran were measured experimentally for the head, beam, and bow oblique waves (Mai et al., 2024). The motion response and vertical acceleration of the ship were also determined according to a ratio of wavelength to ship length of 0.5 to 2.0. The results showed that the ship's response at zero speed was verified by the numerical results obtained from the Ansys AQWA model. Finally, Wu et al. (2021) proposed a control model of a USV catamaran to evaluate the ship's controllability in wind, waves, and currents. They calculated the hydrodynamics, wave forces, and wind forces acting on the ship using empirical formulas.

As can be seen, previous studies mainly focused on the motion and loading of the catamaran at high speed, while some research looked at the development of USV catamarans in ocean waves. This paper combines these efforts, presenting the motion responses and wave-induced shear force and bending moment of a USV catamaran at low speed in water waves through numerical analysis based on Ansys AQWA 2021.

2. MATHEMATICAL MODELING

2.1 Coordinate System and Symbols

A body-fixed coordinate system is used to define the displacement and fluid hydrodynamics acting on the ship. The origin of the coordinate system lies on the horizontal plane of the undisturbed free surface, with the z-axis pointing upward through the center of gravity of the ship and the x-axis pointing toward the bow, as described in Fig. 1.

The ship displacements are defined with the following formula:

$$\vec{X} = [x \quad y \quad z \quad \phi \quad \theta \quad \psi]^T \tag{1}$$

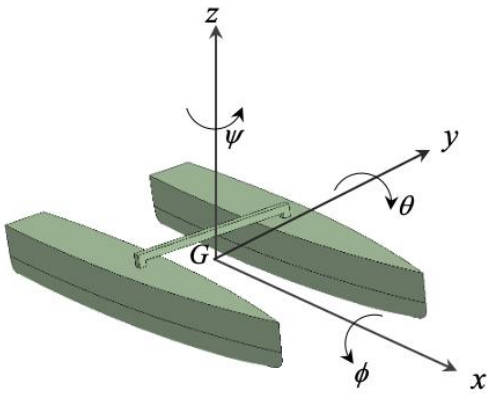

Fig. 1 Definition of coordinate system and symbols

where the ship displacements along the *x*-, *y*-, and *z*-axes are defined as surge, sway, and heave, respectively, and the angular displacement around the corresponding axes are denoted as roll ϕ, pitch θ, and yaw ψ, respectively.

2.2 Numerical Method

The ship's response and bending moment are due to the difference between the ship's load and the water pressure distribution on the ship's surface when the ship operates in both calm water and sea waves. With the designed center of gravity, the water pressure distribution is determined by solving Eq.(2) for the ship motion in waves (Edward, 1989), where M, A_w, B, and C are the inertial mass matrix of the platform, added mass, total damping, and stiffness matrices, respectively, and $F_w(t)$ represents the wave forces acting on the ship over time t.

$$(M + A_w)\ddot{X}(t) + B\dot{X} + CX(t) = F_w(t) \tag{2}$$

Potential flow is often applied to simulate the ship's motion in open water waves for its time efficiency and reasonable accuracy. Following this method, the governing equations and boundary conditions on the free water surface, body surface, bottom of the water area, and zero disturbance in the far-field fluid domain are presented in Eqs. (3)–(7), respectively, where ϕ_I, ϕ_r, and ϕ_d denote the potential of the incident wave, radiation potential velocity, and the diffracted potential velocity, respectively, ω and ω_e are the wave frequency and encounter frequency, respectively.

$$\frac{\partial^2\varphi}{\partial x^2} + \frac{\partial^2\varphi}{\partial y^2} + \frac{\partial^2\varphi}{\partial z^2} = 0 \tag{3}$$

$$-\omega^2\varphi + g\frac{\partial\varphi}{\partial z} = 0 \tag{4}$$

$$\frac{\partial\varphi_r}{\partial n} = -i\omega_e n_j \tag{5}$$

$$\frac{\partial\varphi_d}{\partial n} = -\frac{-\partial\varphi_I}{\partial n} \tag{6}$$

$$\frac{\partial\varphi}{\partial z} = 0 \tag{7}$$

The Green function is adopted to calculate the potential velocities of the diffracted and radiation waves. The first-order hydrodynamic pressure and hydrodynamic forces on the mean wetted surface S_0 of the catamaran due to water waves are then obtained from these potential velocities:

$$p = i\omega\rho\varphi(\vec{x})e^{-i\omega t} \tag{8}$$

$$F_{Ij} = -\rho\int_{S_0} i\omega\varphi_I(\vec{x})n_j dS \tag{9}$$

$$F_{dj} = -i\omega\rho\int_{S_0}\varphi_d(\vec{x})n_j dS \tag{10}$$

$$F_{rjk} = -i\omega\rho\int_{S_0}\varphi_{rk}(\vec{x})n_j dS \tag{11}$$

The response of the ship in regular waves is predicted by solving the ship's equation of motion in the frequency domain, as shown in Eq. (2). The ship's motion in irregular waves is then obtained by integrating the ship response in regular waves over the encountered wave spectrum as shown in Eq. (15). The response variance of the catamaran is then calculated using the last formula. Finally, we determine the significant amplitude of ship motion as twice the root mean square of the response variance.

$$[x_{jm}] = H[F_j] \tag{12}$$

$$H = \{-\omega^2(M_{jk} + A_{jk}) - i\omega B_{jk} + C_{jk}\}^{-1} \tag{13}$$

$$S_\zeta(\omega_e, \mu, U) = S_\zeta(\omega)/|1 - (2\omega U/g)\cos\mu| \tag{14}$$

$$S_j(\omega_e) = |\overline{X_j}(\omega_e, \mu, U)|^2 S_\zeta(\omega_e, \mu, U) \tag{15}$$

$$m_0 = \int_0^\infty \omega_e S_j(\omega_e) d\omega_e \tag{16}$$

where H is the transfer function that relates input forces to output response and $S(\omega_e, \mu, U)$ is the encountered wave spectrum.

The external hydrodynamic force and moment about the neutral axis are calculated as the integral of the pressure field over the wetted surface of the ship. The wave-induced shear force and moment are consequently defined as follows:

$$\overrightarrow{SF}(\omega, X_0) = \iint_{S_0}(-p\vec{n})\,dS \tag{17}$$

$$\overrightarrow{BM}(\omega, X_0) = \iint_{S_0}(\vec{X} - \overrightarrow{X_0}) \times (-p\vec{n})\,dS \tag{18}$$

The obtained shear force and bending moment are then non-dimensionalized using the following equations:

$$F(-) = \frac{SF*L}{\rho\times\nabla\times g\times A} \tag{19}$$

$$M(-) = \frac{BM}{\rho\times\nabla\times g\times A} \tag{20}$$

where ρ, A, g, and ∇ are the seawater density, wave amplitude, gravitational acceleration, and the displaced volume of the ship.

3. Ship Motion in Water Waves

3.1 Main Specification of the Catamaran

A catamaran as a launching and recovery vehicle is selected as the object to predict the ship response and wave load in the present study. The ship mounted with an underwater vehicle travels at 3.0 kn, corresponding to a Froude number of 0.132. The longitudinal center of gravity (LCG) is 5.60 m from the ship's stern, and the vertical center of gravity (VCG) is 1.10 m from the keel.

Table 1 Main parameters of the catamaran

Name	Unit	Value
Length overall L_{OA}	m	12.00
Waterline length L	m	11.91
Beam overall B	m	6.00
Beam demi-hull b	m	1.50
Designed draft T	m	0.65
Distance between the centerline of two hulls H	m	4.50
Displacement D	kgf	16,062
Volume Ñ	m^3	15.67
LCG from AP	m	5.60
VCG	m	1.10
Roll radius of gyration k_{xx}	B	0.28
Pitch radius of gyration k_{yy}	L_{pp}	0.25
Yaw radius of gyration k_{zz}	L_{pp}	0.25
Froude number	-	0.132

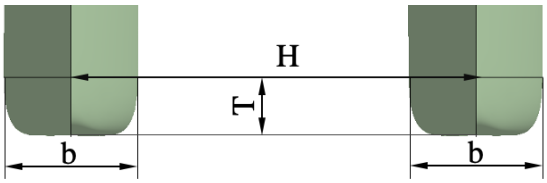

(a) Side view

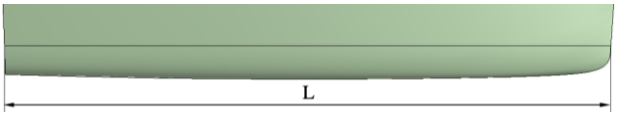

(b) Front view

Fig. 2 Geometry and main dimensions of the catamaran

The main parameters of the model are listed in Table 1. Figure 2 presents an overview and main dimensions of the ship.

First, we conduct a numerical study of the catamaran in head, beam, and 120° and 150° bow oblique waves to predict the responses of heave, roll, and pitch and wave-induced shear force and bending moment of the ship in regular waves. Wavelength-to–ship length ratios (l/L) from 0.4 to 2.0 are considered. Next, we calculate the responses of the heave, roll, and pitch motion of the ship in irregular waves, along with the corresponding shear force and bending moment. Wave frequencies in the force/moment analysis range from 0.1 to 3.0 rad/s for the head and beam waves. The procedure for predicting the ship motion and wave loads is shown in Fig. 3.

3.2 Numerical Setup

We predict the ship's response in regular waves with numerical simulation using Ansys AQWA, applying the boundary element approach to represent the potential flow around the hull. The ship geometry is first simplified to adapt to the simulation environment. Then, a fluid domain with a depth of 20 m and an unrestricted water surface is

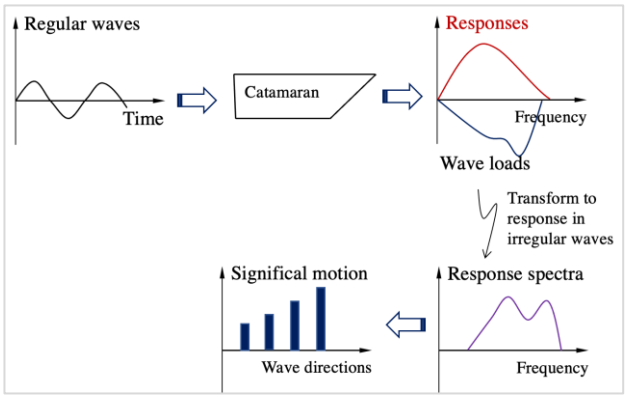

Fig. 3 Numerical prediction of the motion and wave loads of the catamaran

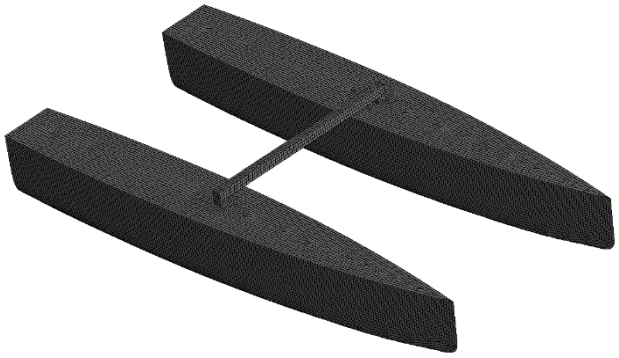

Fig. 4 Mesh on the catamaran

established to simulate the ship in open sea. The ship surface is discretized into elements for both diffracted and non-diffracted domains. The ship speed is set to 1.54 m/s. Figure 4 illustrates the mesh on the surface of the catamaran.

The total number on the catamaran surface is 35,502, 14,466 of which are in the diffracted domain. In addition to regular waves, we study the ship motion in sea states 2 and 3. The ITTC-1978 wave spectrum in sea state 2 and sea state 3 is chosen as the operating environment of the USV catamaran. Figure 5 presents the definition of the wave directions and the wave spectrum density in sea state conditions.

3.3 Ship Response in Water Waves

To evaluate the seakeeping behaviors of the catamaran in sea waves, we predict its motion response characteristics and compare them with the experimental data. The ship responses in regular waves obtained from Ansys AQWA solver for the designed speed are illustrated in Fig.s 6–8 for the heave, roll, and pitch of the catamaran in non-dimensional form, respectively, where k is the wave number. The subfigures a–d present the motion of the catamaran in the water waves with the directions of $\mu = 90°$, 120°, 150°, and 180°, respectively. The numerical results are verified with the experimental data of the same catamaran model in the deep seas (Mai et al., 2024). Here, the RAOs (response amplitude operators) of heave, roll, and pitch agree reasonably well with the

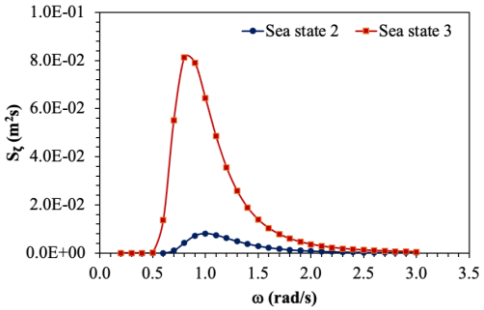

(a) *ITTC-1978 wave spectrum density*

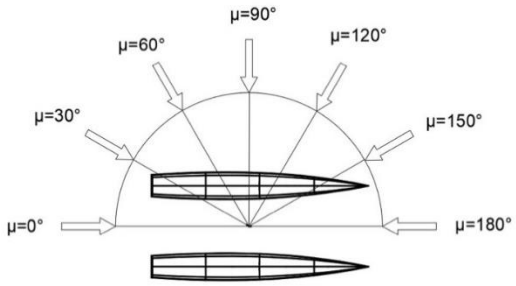

(b) *Wave direction*

Fig. 5 Wave spectrum density and directions

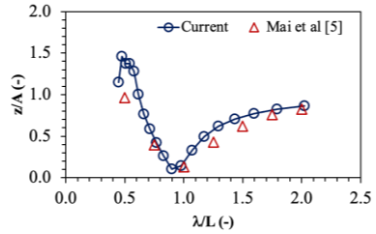

(a) μ= *90 degrees*

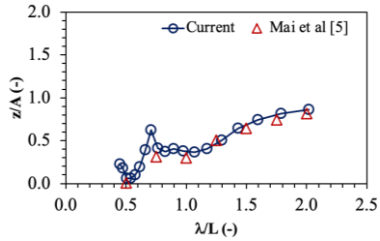

(b) μ= *120 degrees*

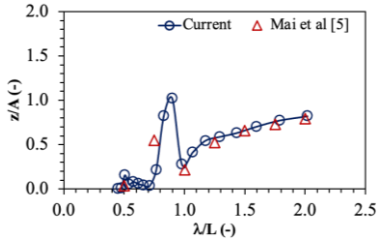

(c) μ= *150 degrees*

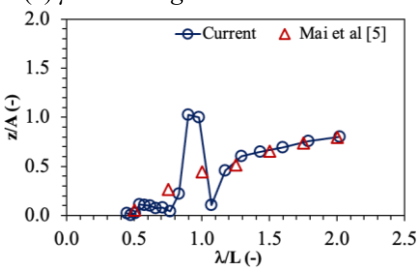

(d) μ= *180 degrees*

Fig. 6 Heave responses of the catamaran in different wave directions

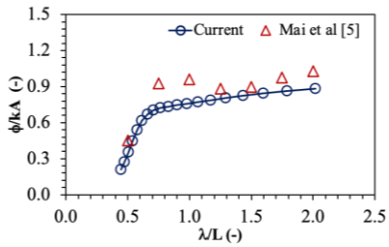

(a) μ= *90 degrees*

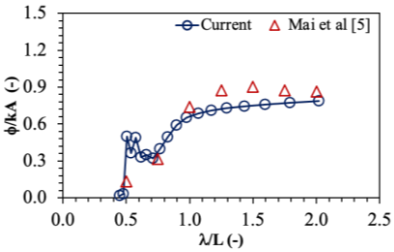

(b) μ= *120 degrees*

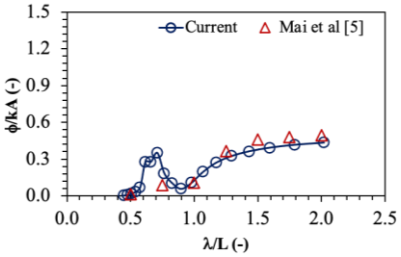

(c) μ= *150 degrees*

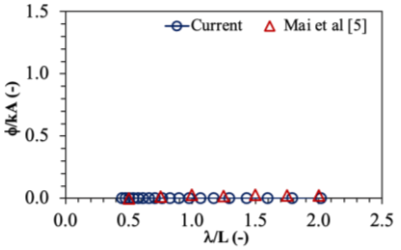

(d) μ= *180 degrees*

Fig. 7 Roll responses of the catamaran in regular waves

corresponding experiment data. However, the pitch responses have a significant difference from experimental results in cases of large wavelengths, where the numerical prediction of the pitch motion is larger than that of experimental measurements.

Figure 6 shows that local maxima of the heave motion are present at λ/L = 0.9 for the cases of the head seas (i.e., 180°) and 150° oblique seas, but a maximum heave response at 120° occurs at λ/L = 0.7. The heave response is approximately zero at λ/L = 0.9 when the catamaran is moving in the beam seas (i.e., 90°), and the maximum heave response for these seas is 1.48.

Figure 7d shows that the roll responses of the ship in head seas are near zero because the frictional force is assumed to be zero with the assumption of invisible flow. The ship's roll in case of beam seas increases as the wavelength-to–ship length ratio increases. A change in slope in the roll response curve in the beam seas can be found at λ/L = 0.6. The maximum local value of the roll occurs at λ/L = 0.7 for the catamaran in bow oblique waves.

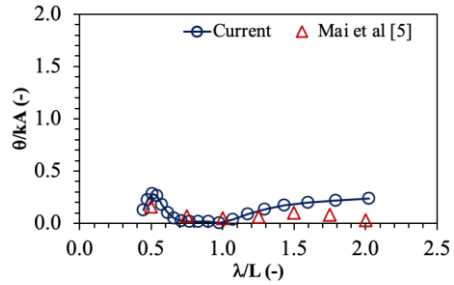

(a) μ= *90 degrees*

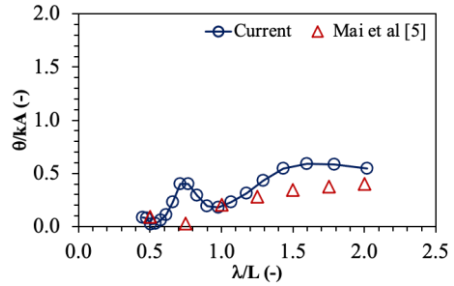

(b) μ= *120 degrees*

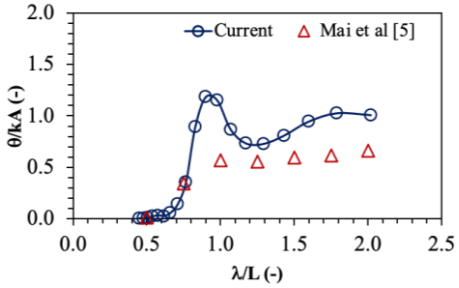

(c) μ= *150 degrees*

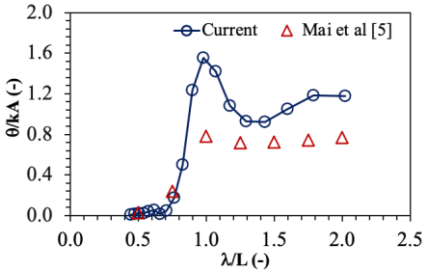

(d) μ= *180 degrees*

Fig. 8 Pitch responses of the catamaran in regular waves

Figure 8 shows that the pitch response becomes very small in the beam seas but is most severe in the head seas. Local maxima are near the resonance condition in Figs. 8c and 8d. The peak pitch response is estimated to be 1.56 in these cases, where the wavelength equals the ship length.

We calculate the ship response in irregular waves by integrating the results of ship motion in regular waves over the wave spectral formula recommended by ITTC-1978 (ITTC, 1978). The catamaran's response to irregular waves is predicted when the ship operates in sea states 2 and 3. Figures 9 and 10 present the responses of heave, roll, and pitch motions of the ship in sea states 2 and 3, respectively. The heave response in irregular beam waves

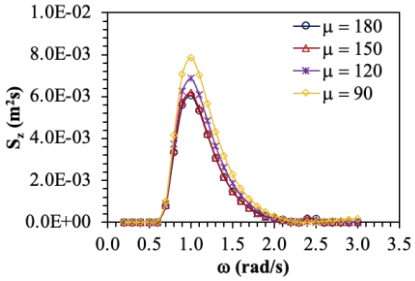

(a) *Heave response to irregular waves*

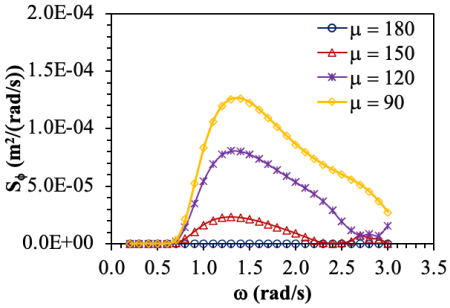

(b) Roll response to irregular waves

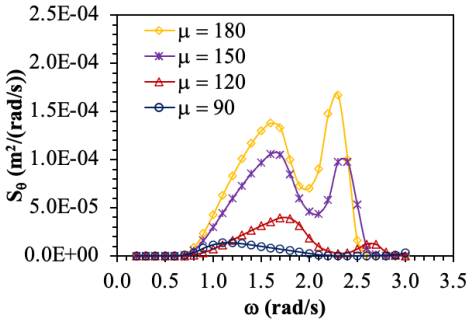

(c) *Pitch response to irregular waves*

Fig. 9 Motion response of the catamaran irregular waves with sea state 2

is larger than that in head waves and oblique waves. The significant heave response in the beam and bow oblique waves may be caused by the increase in ship contact surface and inner region under the impact of the sea waves. The heave response peaks at a wave frequency of 1.0 rad/s, but the roll response peak is 1.1 rad/s. The pitch motion has two local peak values at frequencies of 1.6 and 2.3 rad/s.

In addition, these results show that the wave direction has a significant effect on the roll response to irregular waves, as shown in Fig.s 9b and 10b. The roll responses of the ship in irregular beam sea and oblique seas of 120 degrees are significant. The peak roll responses occur at a wave frequency of 1.3 rad/s for beam and oblique waves.

The pitch responses of the catamaran in irregular waves are illustrated in Fig.s 9c and 10c for sea states 2 and 3, respectively. The local peak values are at frequencies of 1.6 and 2.3 rad/s for the head seas and 150° bow oblique seas, respectively. The ship's response is approximately zero in the frequency ranges of 0.1 to 0.6 rad/s for sea state 2 and 0.1 to 0.5 rad/s for sea state 3. This

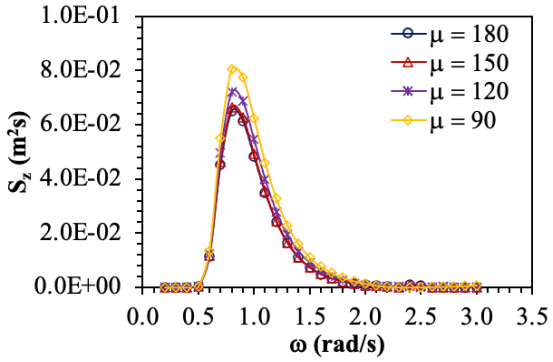

(a) Heave response to irregular waves

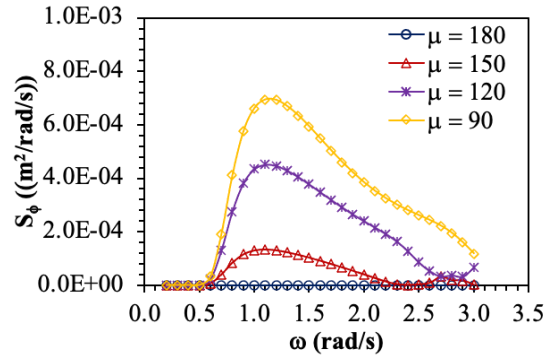

(b) Roll response to irregular waves

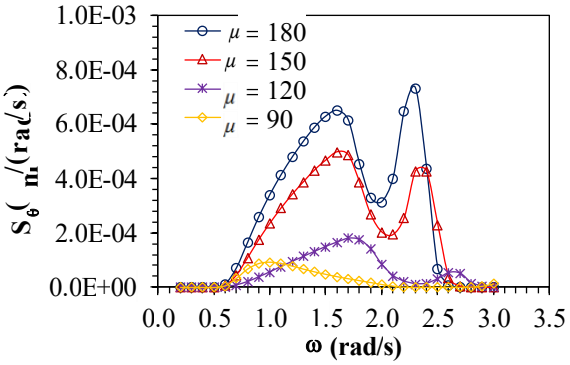

(c) Pitch response to irregular waves

Fig. 10 Motion response of the catamaran irregular waves with sea state 3

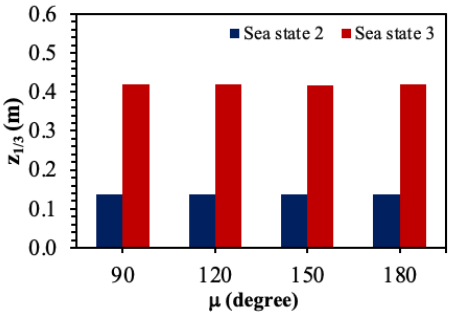

(a) Heave motion

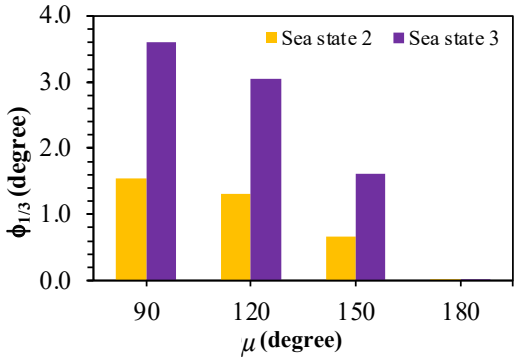

(b) Roll

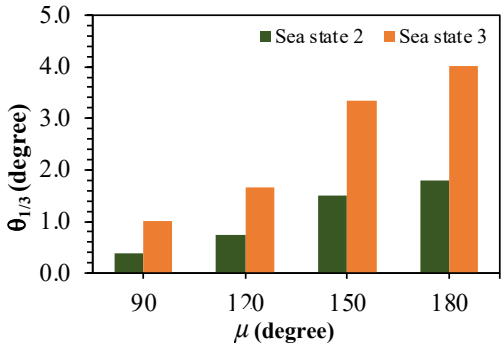

(c) Pitch

Fig. 11 Significant amplitude of heave, roll, and pitch of the ship in sea states 2 and 3

is consistent with the wave spectral density model in the same frequency range.

The calculated significant amplitude of the ship's heave, roll, and pitch responses in the sea states 2 and 3 are shown in Fig. 11. The significant amplitudes of the heave motion in the wave directions are similar. The values for heave and roll are maximum at the wave direction of 90°. This can be explained by the increased difference in dynamic pressure between the two hulls of the catamaran as the ship oscillates in beam waves.

The peak significant amplitudes of the heave approximate 0.138 and 0.42 m when the catamaran operates in sea states 2 and 3, respectively. For the roll motion, the peak values are approximately 1.55 and 3.61 m for the two sea state cases. The significant amplitude of the pitch motion to head waves and 150° bow oblique waves are of concern, peaking at 1.8 and 4.02 m for the cases of the ship in sea states 2 and 3, correspondingly.

4. WAVE LOADS OF THE CATAMARAN

4.1 Wave-Induced Loads Along Ship Length

The wave-induced shear force and bending moment of the ship at different longitudinal positions are analyzed for head and beam waves. The shear force and midship bending moments of the ship are presented as functions of the ratios of wavelength to ship length in Fig.s 12–14. The x-axis in each graph represents the longitudinal position of the catamaran; $x = 0$ corresponds to the center of gravity of the ship, and $x = 0.355$ m represents the position at midship.

The vertical shear forces of the catamaran in regular waves are larger for the head waves than for the beam

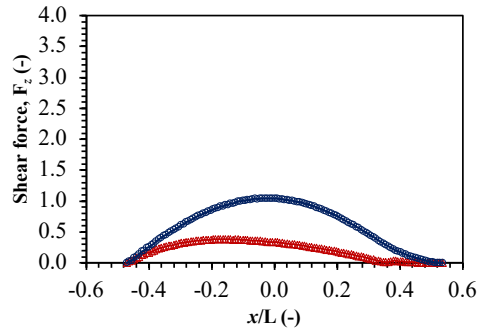

(a) $\mu = 90^o$

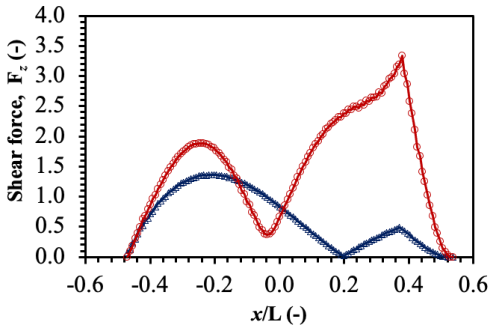

(b) $\mu = 180^o$

Fig. 12 Vertical shear force of the ship in beam seas and head seas: λ/L=2.0 (blue) and λ/L=1.0 (red)

waves, as shown in Fig. 12. The blue and red symbols in the figures indicate the ratios of wavelength to ship length as 2.0 and 1.0, respectively. In the head seas, the shear force in regular waves with $\lambda/L = 1.0$ is larger than that with $\lambda/L = 2.0$. The peak values of the dimensionless shear forces in head seas at ¼L and ¾L positions from the stern of the ship are estimated to be 1.71 and 2.54, respectively, for $\lambda/L = 1.0$. On the other hand, the shear force of the ship at ¾L is quite small for $\lambda/L = 2.0$ but predicted to be 1.39 at ¼L.

The midship transverse bending moment of the ship in the head sea and beam sea cases are illustrated in Fig. 13. This moment in the head seas is very small and, thus, ignored. Meanwhile, the transverse bending moment at midship should be considered when studying the strength of the ship in the beam seas. The peak values of the midship bending moments of the ship in beam seas are approximately 0.0091 and 0.0156 for $\lambda/L = 2.0$ and $\lambda/L = 1.0$. The bending moment is significant in a wide range of wave frequencies.

The variation of the midship vertical bending moment of the catamaran is illustrated in Fig. 14. This bending moment in the head seas for $\lambda/L = 1.0$ is the largest when compared to the other cases, with a peak value of 6.4. For the beam seas, the midship vertical bending moment caused by the waves is quite small compared to the corresponding vertical bending moment. This can be explained by the small vertical pressure induced by the beam waves in this case.

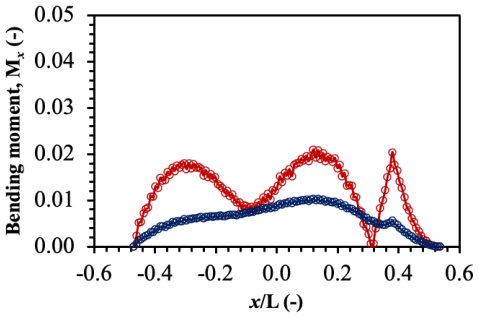

(a) $\mu = 90^o$

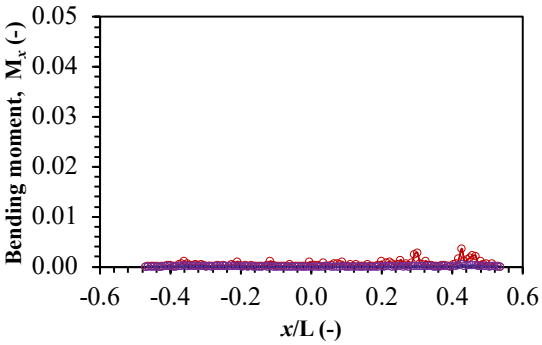

(b) $\mu = 180^o$

Fig. 13 Transverse bending moment of the ship in beam seas: λ/L = 2.0 (blue); λ/L = 1.0 (red).

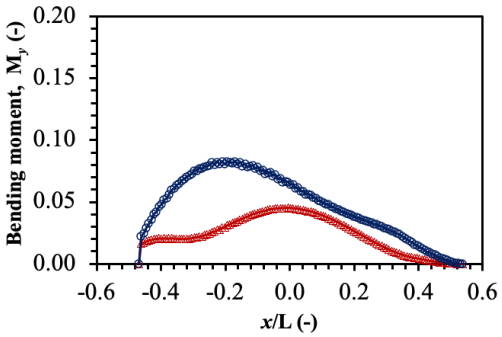

(a) $\mu = 90^o$

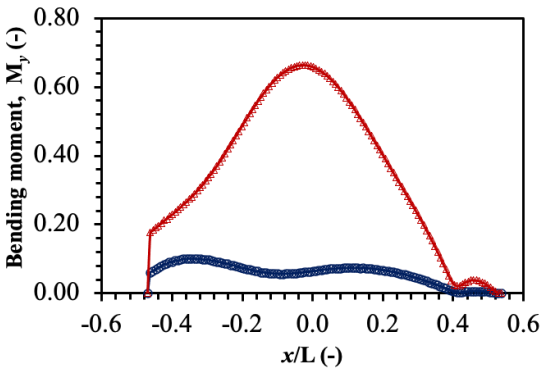

(b) $\mu = 180^o$

Fig. 14 Vertical bending moment of the ship in beam seas and head sea: λ/L=2.0 (blue); λ/L=1.0 (red)

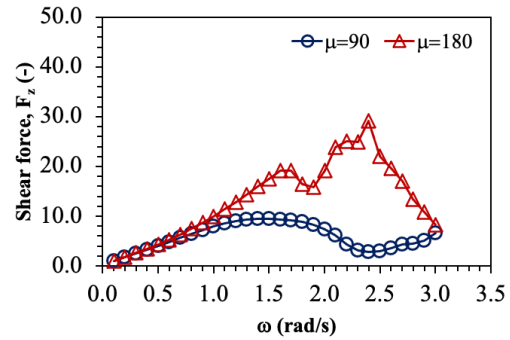

(a) *At ¼L from the stern*

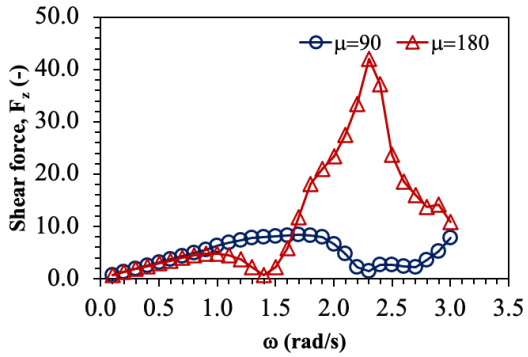

(b) *At ¾L from the stern*

Fig. 15 Variation in vertical shear force as a function of wavelength or wave frequency

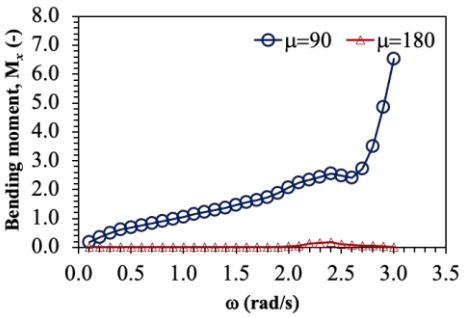

Fig. 16 Midship transverse bending moment as a function of wave frequency

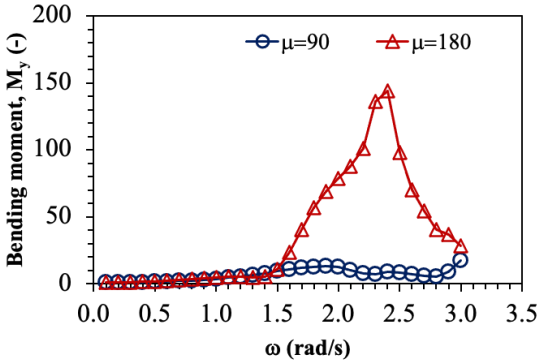

Fig. 17 Midship vertical bending moment as a function of wave frequency

4.2 Wave-induced Loads as Functions of the Wave Frequency

Figures 15–17 show the wave-induced shear force and midship transverse and vertical bending moments, respectively, of the catamaran as functions of wave frequency of the head waves and beam waves. These values are quite small when the ship moves in long waves (e.g., $\omega < 1$ rad/s). Figure 15 illustrates the wave-induced shear force at ¼*L* and ¾*L* from the stern. The vertical shear force of the ship in head seas is significantly larger than that in the beam seas. The peak shear force at ¾*L* from the stern is estimated to be approximately 42, but it is also significant at ¼*L* across the frequency domain. This can be explained by the increased effect of water waves on the inner region of the catamaran when the ship moves in beam waves.

The midship transverse bending moment is maximum in beam seas and close to zero in head waves, as shown in Fig. 16. This moment increases linearly in long waves of 0.1 to 1.9 rad/s and then increases sharply with wave frequencies from 2.7 to 3.0 rad/s. Therefore, the bending moment induced by water waves has a dramatic effect on the ship's strength.

Figure 17 illustrates that the midship vertical bending moment as a function of the wave frequency in the head seas is much larger than in beam seas. The peak value is approximately 144.8 for the wave frequency of 2.4 rad/s but approximately zero in the frequency range from 0.1 to 1.4 rad/s.

5. CONCLUSION

The paper presents the numerical estimation of the responses, wave-induced shear force, and bending moment of a low-speed catamaran in water waves in various directions using Ansys AQWA. The responses of the catamaran include heave, roll, and pitch in head, beam, and bow oblique waves of 120° and 150° at λ/L values of 0.45 to 2.0. Additionally, the vertical shear force and bending moment of the *x*- and *y*-axes caused by the head waves and beam waves are analyzed.

The results of the ship responses are in agreement with the experimental data. In addition, the results of the significant amplitudes of the ship's roll, pitch, and heave in sea states 2 and 3 indicate that the heave and roll of the ship in beam waves and oblique waves should be taken into account. Meanwhile, the pitch of the ship in the head waves and the oblique waves of 150 degrees is larger than those in the other cases. In addition, the significant amplitudes of the heave, roll, and pitch are predicted when the USV catamaran operates in sea states 2 and 3.

The maximum shear forces of the *z*-axis occur when the ship moves in head seas. The maximum shear forces at ¼*L* and ¾*L* from the stern are approximately 1.74 and 2.54 for $\lambda/L = 1.0$. The maximum midship transverse bending moment is approximately 0.0156 for the case of the ship in beam seas and is very small for the case of the ship in head seas. Additionally, the shear force at positions ¼*L* and ¾*L* from the stern of the ship and midship bending

moment as a function of wave frequency are also evaluated. The vertical shear force and vertical bending moment are significant in the wave frequency range from 1.5 to 3.0 rad/s. However, the midship transverse bending moment is significant over the entire wave frequency range. The longitudinal and transverse strengths of the USV catamaran under the effect of the water waves should be evaluated in the further study.

CONFLICT OF INTEREST

The authors declare no conflicts of interest.

AUTHORS CONTRIBUTION

T. T. Nguyen: Conceptualization, Methodology, Software, Validation, writing—original draft; **T. L. Phan**: Formal analysis, Investigation, Validation, Writing – review & editing; **T. H. Le**: Validation, Writing – review & editing.

REFERENCES

Armstrong, T. & Schmieman, A. (2005, June 27–30). On the Added Resistance of Catamarans in Waves *International Conference on Fast Sea Transportation*. Saint Petersburg, Russia. https://repository.tudelft.nl/record/uuid:978c653e-efae-4fa3-838d-847f1f128443.

Bouscasse, B., Broglia R., & Stern, F. (2013). Experimental investigation of a fast catamaran in head waves. *Journal of Ocean Engineering*, *72*, 318–330. https://doi.org/10.1016/j.oceaneng.2013.07.012.

Durante, D., Broglia, R., Diez, M., Olivieri, A., Campana, E. F., & Stern, F. (2020). Accurate experimental benchmark study of a catamaran in regular and irregular head waves including uncertainty quantification. *Journal of Ocean Engineering*, *195*, 1–21, 2020. https://doi.org/10.1016/j.oceaneng.2019.106685.

Edward, V. L. (1989). *Introduction to Naval Architecture*, SNAME. https://navalifpe.wordpress.com/wpcontent/uploads/2011/09/principles-of-naval-architecture-vol-1-sname.pdf.

Fang, C. C., & Chan, H. S. (2004). Investigation of seakeeping characteristics of high-speed catamarans in waves. *Journal of Marine Science and Technology*, *12*(1), 7–15. https://doi.org/10.51400/2709-6998.2215.

Fitriadhy, A., Razali, N. S., AqilahMansor, N. (2017). Seakeeping performance of a rounded hull catamaran in waves using CFD approach. *Journal of Mechanical Engineering and Sciences*, *11*(2), 2601–2614. http://dx.doi.org/10.15282/jmes.11.2.2017.4.0238.

Guo, Z., Ma, Q., & Hu, X. (2016). Seakeeping analysis of a wave-piercing catamaran using URANS-based Method. *International Journal of Offshore and Polar Engineering*, *26*(1), 48–56. https://doi.org/10.17736/ijope.2016.mk38.

Huang, S., Liu, W., Luo, W., & Wang, K. (2021). Numerical simulation of the motion of a large scale unmanned surface vessel in high sea state waves. *Journal of Marine Science and Engineering*, *9*(982), 1–22. https://doi.org/10.3390/jmse9090982.

ITTC (1978). Report of seakeeping committee. https://ittc.info/media/2214/report-of-seakeeping-committee.pdf.

Lin, C. T. (2017, November 5–8). *Investigation of the Seakeeping Performance of Twin Hull Vessels by Different Computational Methods* [10th International Workshop on Ship and Marine Hydrodynamics]. Keelung, Taiwan, China. https://www.semanticscholar.org/paper/Investigation-of-the-Seakeeping-Performance-of-Twin-Lin-Lin/139b197b20b9bfdfe90d3ed7f2a2ad02634ff423.

Liu, M. (2016). *Experimental and numerical studies of hydrodynamic interaction of two bodies in waves. Motion Data of Model in Two-body Case* [Master thesis] https://research.library.mun.ca/12154/1/thesis.pdf.

Mai, T. L., Vo, A. K., Cho, A., Mai, V. T., & Yoon, H. K. (2024). Experimental investigation on wave characteristics due to interference of catamaran demi-hulls in waves. *International Journal of Naval Architecture and Ocean Engineering, 9*(3), 1-24. 2024. https://doi.org/10.1016/j.ijnaoe.2024.100594.

Matsubara, S (2011). *Ship motions and wave-induced loads on high speed catamarans* [PhD thesis]. https://figshare.utas.edu.au/articles/thesis/Ship_motions_and_wave-induced_loads_on_high_speed_catamarans_/23208470?file=40905524.

Novák, F. (2022). *State estimation of an unmanned surface vehicle by an unmanned multirotor helicopters. Estimation of USV states using Linear Kalman filter.* [Master's Thesis]. https://dspace.cvut.cz/bitstream/handle/10467/100876/F3-DP-2022-Novak-Filip-master_thesis.pdf.

Sun, H., Jing, F., Jiang, Y., Zou, J., Zhuang, J., & Ma, W. (2016). Motion prediction of catamaran with a semisubmersible bow in wave. *Journal of Polish Maritime Research*, *23*, 37–44. https://doi.org/10.1515/pomr-2016-0006.

Vernengo, G., Villa, D., Bruzzone, D., & Bonfiglio, L. (2021). A study on the added resistance of a catamaran advancing in waves considering variations of both operating and geometric parameters. *Journal of Ships and Offshore Structures*, *16*(4), 334–352. https://doi.org/10.1080/17445302.2020.1727180.

Wang, X., Liu, L., Zhang, Z., & Feng, D. (2020). Numerical study of the stern flap effect on catamaran' seakeeping characteristic in regular head waves. *Journal of Ocean Engineering, 206*, 1–14. https://doi.org/10.1016/j.oceaneng.2020.107172.

Wu, G., Zhao, M., Cong, Y., Hu, Z., & Li, G. (2021). Algorithm of berthing and maneuvering for

catamaran unmanned surface vehicle based on ship maneuverability. *Journal of Marine Science and Engineering*, *9*(3), 1–24. https://doi.org/10.3390/jmse9030289.

Zaraphonities, G., Grigoropoulos, G. J., Damala, D. P., & Mourkoyannis, D. (2015). Seakeeping analysis of two medium-speed twin-hull models. *Journal of Ship Production and Design*, *31*(3), 192-200. https://doi.org/10.5957/jspd.2015.31.3.192.

Zhang, W., Li, Y., Liao, Y., Jia, Q., & Pan, K. (2021). Hydrodynamic analysis of self-propulsion performance of wave-driven catamaran. *Journal of Marine Science and Engineering*, *9*(1221), 1–31. http://dx.doi.org/10.3390/jmse9111221.